ORIGINAL PAPER

Control of buoyant flow and heat dissipation in a porous annular chamber using a thin baffle

B V Pushpa[1], Y Do[2] and M Sankar[3,4]*

[1]Department of Mathematics, BMS Institute of Technology and Management, Bengaluru 560064, India

[2]Department of Mathematics, KNU-Center for Nonlinear Dynamics, Kyungpook National University, Daegu 41566, Republic of Korea

[3]Faculty of Mathematics, General Requirements Department, University of Technology and Applied Sciences (CAS-Ibri), P. O. Box 14, 516 Ibri, Oman

[4]Department of Mathematics, School of Engineering, Presidency University, Bengaluru 560064, India

Abstract: This paper reports the numerical simulations on buoyant thermal transfer inside the finite porous cylindrical annular region with a thin circular baffle attached to inner cylinder. The main objective of this investigation is to provide a detailed impact of baffle on flow and heat transport rates due to the direct relevance of this problem to the design of heat exchangers. The side walls of annular enclosure are maintained at uniform, but different temperatures, while the top and bottom walls are insulated. The Brinkman-extended Darcy model is adopted for the momentum equations, and simulations of the governing PDEs are performed using the ADI and SLOR algorithms. The predictions from the present simulations detected that the size and position of baffle has predominant impact on buoyant flow and thermal transport characteristics. It has been detected that the thermal dissipation rates could be enhanced by positioning the baffle near the upper boundary, while increasing the baffle length leads to the reduction of thermal transport. The size and location of baffle emerges out as an important quantity in regulating the global thermal transfer through modifying the flow regimes in the annular geometry. Interestingly, the magnitude of flow circulation enhances with an increase in Rayleigh and Darcy numbers for any baffle length and position.

Abbreviations

A	Aspect ratio
c_p	Specific heat at constant pressure
D	Width of the annulus (m)
Da	Darcy number
g	Acceleration due to gravity (m/s^2)
H	Height of the annulus (m)
h	Dimensional location of baffle (m)
K	Permeability of the porous medium (m^2)
k	Thermal conductivity (W/(m K))
l	Dimensional length of baffle (m)
L	Dimensionless location of the baffle
$\overline{Nu}$	Average Nusselt number
p	Fluid pressure (Pa)
Pr	Prandtl number
Ra	Thermal Rayleigh number

Ra_D	Darcy-Rayleigh number $\left(Ra_D = \frac{gK\beta_T(\theta_h-\theta_c)D^2}{\upsilon k\alpha}\right)$
T	Dimensionless temperature
t*	Dimensional time (s)
t	Dimensionless time
(r_i, r_o)	Radius of inner and outer cylinders (m)
(r, z)	Dimensional radial and axial co-ordinates (m)
(R, Z)	Dimensionless radial and axial co-ordinates
(u, w)	Dimensional velocity components in (r, z) directions (m/s)
(U, W)	Dimensionless velocity components in (R, Z) directions

Greek letters

α	Thermal diffusivity (m^2/s)
β	Thermal expansion coefficient (1/K)
ε	Dimensionless length of baffle
ζ	Dimensionless vorticity
θ	Dimensional temperature (K)
λ	Radius ratio

*Corresponding author, E-mail: manisankariyer@gmail.com

υ   Kinematic viscosity (m^2/s)
ρ   Fluid density (kg/m^3)
φ   Porosity of the porous medium
ψ   Dimensionless stream function

1. Introduction

Convection in a differentially heated vertical annular space with hot and cold vertical walls and insulated top and bottom boundaries forms an important model problem in many applications, such as heat transfer equipment, nuclear systems, crystal growth processes and has also been widely investigated. The first extensive numerical investigation on buoyant convective flow in a vertical annulus with differently heated vertical cylinders and horizontal adiabatic boundaries by de Vahl Davis and Thomas [1] using finite difference technique. Venkatachalappa et al. [2] performed numerical simulations in an annular space having rotating inner and outer walls and observed higher heat transfer rate for rotating walls as compared to stationary boundaries. Mebarek-Oudina [3] presented numerical results on hydrodynamic stability in an annulus having thermal sources of different length. The collective impacts of magnetic and/or thermocapillary forces on buoyant motion inside the annular domain are analyzed and brought out the detailed impacts of magnetic and thermocapillary forces [4–6]. Zhang et al. [7] performed two- and three-dimensional study on buoyant flow and thermal process inside the annular region with slots along inner cylinder. Some of the recent studies on buoyant transport processes in annular domains by considering thermal / solutal sources and sinks has revealed the impacts of discrete sources on the flow and thermal pattern as well as thermal dissipation rates [8, 9]. The above-mentioned works mainly deal with the flow and thermal transport analysis of different fluids in vertical annular geometries without baffle.

Theoreticians and experimentalists have shown that the thermal transport rate can be efficiently controlled by altering the flow patterns in an enclosure and is effectively achieved by placing baffles to one or more thermally active boundaries. Shi and Khodadadi [10] analyzed the impact of a baffle in a rectangular geometry by considering different fin location and size and predicted the significant influences of fin on the flow patterns and thermal transport rates. Later, Tasnim and Collins [11] performed numerical investigation in a square geometry to determine the effects of hot baffle on the buoyant flow and heat transport. Oztop et al. [12] inspected the impacts of a hot plate on buoyant motion in a square cavity and illustrated the predominant

impacts of plate locations on thermal transport rates. Bilgen [13] investigated buoyant motion in a square geometry by considering baffle conductivity. Ben-Nakhi and Chamkha [14, 15] performed numerical analysis to comprehend the influence of an inclined fin on buoyant thermal transport in square geometry by considering the thickness of fin. They revealed the vital impact of fin positions on the flow distribution and the thermal transport. The effect of mutually orthogonal heated baffles on convection heat transfer is numerically examined in a square enclosure by Kandaswamy and co-workers [16, 17] and found that the baffle dimensions strongly influence the flow and thermal distributions. Hussain et al. [18] reported the effect of a tilted baffle on convection heat transfer in a corrugated square cavity. Using Z-shaped baffles, Sriromreun et al. [19] conducted experimental and theoretical investigations in a channel and uncovered the effects of baffle shape on heat transfer enhancement. Wang et al. [20] numerically examined the buoyant convection in a tilted lid-driven square geometry having a thin hot plate and noticed an enhanced thermal transport for vertical positioning of the plate. The combined effects of partition and transverse baffles on natural convection in a ventilated square enclosure has been analyzed by Kalidasan et al. [21] using finite difference method. It is worth to mention that the above studies focus on the impacts of baffle size and position in rectangular and non-rectangular geometries. The baffle impact on thermosolutal convection in an annular geometry is presented by Pushpa et al. [22] by covering a vast range of parametric values. Recently, Girish et al. [23] performed numerical simulations to understand different arrangements of unheated entry and exit on mixed convection flow in an open double-passage annular channel and also observed baffle position is a crucial parameter in altering thermal transport in the channel.

Buoyant convection in porous geometries is found in many industrial setups, namely solar energy collection systems, geothermal applications and building insulation materials. Natural convection in a vertical annular space containing porous materials has been examined experimentally by numerous researchers [24, 25]. Prasad [26] performed numerical simulations of convective transport in a porous annular space by considering isothermal and isoflux heating of inner cylinder. Later, Shivakumara et al. [27] made convective transport analysis in a porous annulus by including the Brinkman and Darcy terms. For a porous annulus space, Sankar et al. [28] examined convective flow and transport processes from a discrete heat source attached to the inner wall and predicted that the heat source positioned nearer to bottom boundary produces maximum heat transport rather than other locations. Recently, Olfian et al. [29] executed numerical experiments of buoyant thermal transport with two different baffle

shapes in the solar heater channel. The influence of porosity combined with thermal radiation and heat generation in a square porous enclosure has also been investigated using different porous media models [30, 31]. Sankar et al. [32] analyzed buoyancy-driven convection due to two thermal sources located along the inner cylinder of an upright porous annular geometry and found that the bottom heater dissipates higher heat than the top heater. Mahapatra and co-workers [33–35] have analyzed the porosity effects in a lid-driven enclosure by considering different effects, such as thermal radiation, non-uniform temperature and cavity inclination. Recently, attention has also been focused on analyzing the impacts of buoyant motion and thermal dissipation rates of nanofluids in finite geometries of different shapes [36–38]. Mondal and Sibanda [39] examined the influence of non-uniform thermal conditions on transient thermosolutal convection in a porous enclosure and proposed heat transfer correlations. Applying FDM, Varol et al. [40] analyzed free convection in a porous triangular cavity having a thin adiabatic fin attached to a boundary. The results reveal that the location, height and width of the fin has significant effect on natural convection. Khanafer et al. [41] used a porous baffle to control buoyant flow in a square geometry and identified an ideal combination of fin position and angle to achieve enhanced thermal transport. In recent years, utilizing different shaped baffle, many researchers analyzed various ways to control the convective flow and associated thermal transport in different geometries representing various heat exchanger applications [42–45]. The above-mentioned investigations mainly analyze the effect of porosity in an annular or square geometry or baffle in a rectangular porous enclosure.

A complete and thorough literature survey has been performed on buoyancy-driven convection in a finite enclosure with a baffle attached to one of the enclosure walls. However, the prevailing studies apparently reveal that the impact of baffle is restricted mainly to square and non-annular geometries. Nevertheless, the consequence of a baffle on buoyant-driven transport processes is not attempted in the earlier studies on similar geometry. The physical geometry considered in this analysis has relevance to heat exchangers [46–49], which are utilized for thermal transport among different fluids used in the system. Heat exchangers are widely used in air conditioning, refrigerators, power stations and petrochemical plants. The main purpose of the design of heat exchangers is to maximize the surface area and minimize the resistance to fluid flow. In heat exchangers, fins or baffles are commonly placed to maintain different flow regimes and to control heat transfer. Realizing this essential application, the main objective of current investigation is to establish a strong basic understanding of the impacts of length and placement of a

circular baffle on buoyant flow and associated transport processes in a cylindrical porous annular enclosure. The Brinkman-extended Darcy model is adopted in the study, and the detailed numerical simulations are obtained to depict the various effects of baffle location and size on buoyant flow and thermal transport processes.

2. Model equations and auxiliary conditions

The geometrical configuration chosen in the present investigation, depicted in Fig. 1, is a vertical annular region formed by two co-axial cylinders of inner radius r_i and outer radius r_o having annular thickness D and elevation H. The annulus is packed with the fluid-saturated porous medium, and the flow is assumed to be axisymmetric. A two-dimensional thin circular conductive baffle of size l is fixed along the inner cylinder. The horizontal boundaries are treated to be insulators, the inner tube is heated (θ_h) and outer tube is cooled (θ_c). Also, the thermal condition of baffle is assumed to be that of inner cylinder. In addition, Newtonian fluid with non-varying properties is presumed except the incorporation of Boussinesq approximation in the axial momentum balance equation. Further, viscous dissipation effects are neglected and gravity direction is taken in the opposite z-axis.

The widely used models in the literature to study the flow problems in porous media are the Darcy model, the Darcy–Brinkman model and the Darcy–Brinkman–Forchheimer models. Apart from these models, the Brinkman-extended Darcy model with the convective terms has also been extensively used in modeling the flow and heat transfer in finite porous enclosures. In the present study, the Brinkman-extended Darcy model with the inclusion of convective and transient terms has been adopted in the governing equations of the problem. The Forchheimer inertia term in the momentum equations is neglected and is more important for non-Darcy effect on the convective boundary layer flow over the surface of a body embedded in a high porosity media. The Brinkman-extended Darcy model, adopted in the present study, has been used in a large number of investigations for natural convection in annular and rectangular porous enclosures. By applying the above assumptions, the equations governing the conservation of mass, momentum and energy are [25–28]:

$$\frac{\partial u}{\partial r} + \frac{\partial w}{\partial z} + \frac{u}{r} = 0, \tag{1}$$

$$\frac{1}{\phi}\frac{\partial u}{\partial t^*} + \frac{1}{\phi^2}\left[u\frac{\partial u}{\partial r} + w\frac{\partial u}{\partial z}\right] = -\frac{1}{\rho_0}\frac{\partial p}{\partial r} + \frac{v}{\phi}\left[\nabla_1^2 u - \frac{u}{r^2}\right] \\ - \frac{v}{K}u, \tag{2}$$
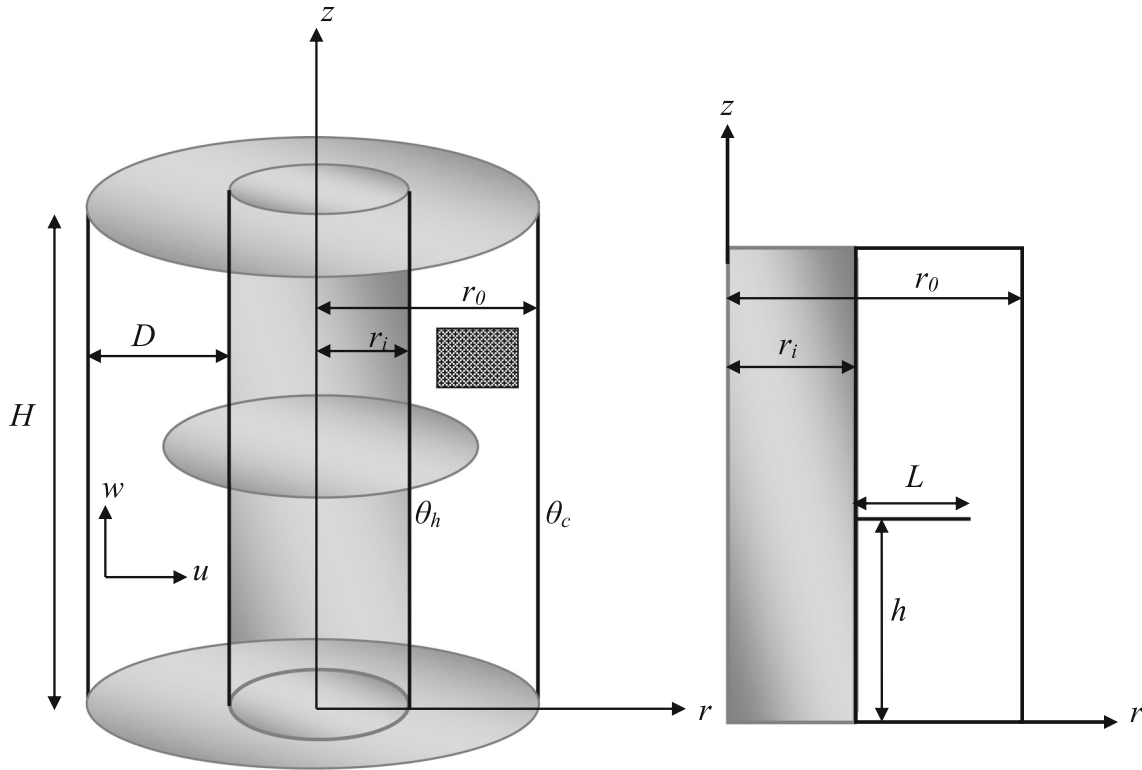
Fig. 1 Physical geometry and axisymmetric structure of the annular domain

$$\frac{1}{\phi}\frac{\partial w}{\partial t^*} + \frac{1}{\phi^2}\left[u\frac{\partial w}{\partial r} + w\frac{\partial w}{\partial z}\right] = -\frac{1}{\rho_0}\frac{\partial p}{\partial z} + \frac{v}{\phi}\nabla_1^2 w + g\beta(\theta - \theta_h) - \frac{v}{K}w,$$

(3)

$$\frac{\partial\theta}{\partial t^*} + u\frac{\partial\theta}{\partial r} + w\frac{\partial\theta}{\partial z} = \alpha\nabla_1^2\theta,$$

(4)

where $\nabla_1^2 = \frac{\partial^2}{\partial r^2} + \frac{1}{r}\frac{\partial}{\partial r} + \frac{\partial^2}{\partial z^2}$,

The following transformations are considered in this study for non-dimensional process:

Annular width D for space variables, (D^2/α) for time, (α/D) for velocity, $\Delta\theta$ for temperature, $(\rho_0\alpha^2/D^2)$ for pressure (α/D^2) for vorticity. Here $D = r_o - r_i$, $\Delta\theta = \theta_h - \theta_c$.

The resulting non-dimensional governing equations after eliminating the pressure term (using cross differentiation) from Eqs. (2) and (3) are [28, 32]

$$\frac{\partial T}{\partial t} + U\frac{\partial T}{\partial R} + W\frac{\partial T}{\partial Z} = \nabla^2 T$$

(5)

$$\frac{1}{\phi}\frac{\partial\zeta}{\partial t} + \frac{1}{\phi^2}\left[U\frac{\partial\zeta}{\partial R} + W\frac{\partial\zeta}{\partial Z} - \frac{U\zeta}{R}\right]$$
$$= \frac{Pr}{\phi}\left[\nabla^2\zeta - \frac{\zeta}{R^2}\right] - \frac{Pr}{Da}\zeta - Pr\,Ra\frac{\partial T}{\partial R}$$

(6)

$$\zeta = \frac{1}{R}\left[\frac{\partial^2\psi}{\partial R^2} - \frac{1}{R}\frac{\partial\psi}{\partial R} + \frac{\partial^2\psi}{\partial Z^2}\right]$$

(7)

$$U = \frac{1}{R}\frac{\partial\psi}{\partial Z}, \qquad W = -\frac{1}{R}\frac{\partial\psi}{\partial R}$$

(8)

where $\nabla^2 = \frac{\partial^2}{\partial R^2} + \frac{1}{R}\frac{\partial}{\partial R} + \frac{\partial^2}{\partial Z^2}$.

The following seven dimensionless parameters arise in the present study (four geometrical and three physical parameters):

$\lambda = \frac{r_0}{r_i}$ radius ratio, $A = \frac{H}{D}$ aspect ratio, $\varepsilon = \frac{l}{D}$ baffle length, $L = \frac{h}{H}$ baffle location, $Pr = \frac{v}{\alpha}$ Prandtl number, $Da = \frac{K}{D^2}$ Darcy number and $Ra = \frac{g\beta(\theta_h-\theta_c)D^3}{v\alpha}$ Rayleigh number.

The dimensionless auxiliary conditions are [10, 11]:

$t = 0:$ $U = W = T = 0, \psi = \zeta = 0$

$t > 0:$ $\psi = \frac{\partial\psi}{\partial R} = 0, T = 1;$ Along inner cylinder

$\psi = \frac{\partial\psi}{\partial R} = 0, T = 0;$ Along outer cylinder

$\psi = \frac{\partial\psi}{\partial Z} = 0, \frac{\partial T}{\partial Z} = 0;$ Along top and bottom walls

$\psi = \frac{\partial\psi}{\partial Z} = 0, T = 1;$ On the baffle.

(9)

The expression for wall vorticity can be derived using the Taylor's series expansion of wall stream function values and interior values of ψ. In this paper, the boundary

vorticity is calculated from the relation: $\zeta_b = \frac{8\psi_{b+1} - \psi_{b+2}}{2(\Delta\eta)^2}$, where b indicates the value of ζ at boundary and $\Delta\eta$ is the spacing between two grid points. In heat transport analysis, the design engineer is interested to investigate the qualitative and quantitative information on the chosen problem. After obtaining the steady-state solutions from the governing Eqs. (6)–(9), the parameter of quantitative interest is the thermal transport rate and is estimated from the local (Nu) and overall ($\overline{Nu}$) Nusselt numbers, given by

$$Nu = \frac{hD}{k} = \frac{q_b D}{k(\theta_h - \theta_c)} = -\frac{\partial T}{\partial R} \text{ and } \overline{Nu} = \frac{1}{A}\int_0^A Nu\, dZ.$$

3. Numerical method and validation

To perform the detailed analysis of the chosen problem, the physical laws are transformed to a system of partial differential equations (PDEs). Since the model equations are coupled and nonlinear, analytical solutions to these equations are not possible. Hence, by utilizing the available high-speed computing resources, the governing partial differential equations are solved numerically using FDM, namely the Alternating Direction Implicit (ADI) and Successive Line Over Relaxation (SLOR) methods. In particular, transient PDEs are discretized by the ADI method. However, vorticity-stream function relation is discretized by SLOR method with proper choice of relaxation parameter. The average Nusselt number is estimated through numerically integrating $\overline{Nu}$. Further, to solve the finite difference equations arising from the discretization process, an in-house code is written and our results are compared with the existing standard benchmark predictions prior to present simulations. The iteration procedure used to find the steady-state solutions for all variables is performed till the below mentioned convergence condition is fulfilled:

$$\max\left[\frac{\left|\chi_{i,j}^{n+1} - \chi_{i,j}^{n}\right|}{\left|\chi_{i,j}^{n+1}\right|}\right] \leq \varepsilon$$

In the above condition, χ stands for T, where i, j denote the grid locations, n represents the time iteration and ε is the convergence criterion. The detailed information on numerical method is provided in our earlier works [6, 9, 33] and are not provided here for brevity.

3.1. Grid sensitivity analysis and validation

All simulations are thoroughly tested for independency of grid sizes by generating uniform grids in the annular domain. To check the grid independency, the average

Table 1 Grid independence results for $Ra = 10^6, Da = 10^{-2}$, $\lambda = 2$, L = 0.5 and $\varepsilon = 0.5$

| Grid size	$\overline{Nu}$	Relative difference
51×51	7.6764	–
81×81	7.4412	0.0315
101×101	7.3456	0.0134
121×121	7.3441	0.0002

Nusselt numbers ($\overline{Nu}$) are obtained by employing different grid sizes. The uniform meshes employed in the present study are: 51×51, 81×81, 101×101 and 121×121. The results for the case of $Ra = 10^6, Da = 10^{-2}$, $\lambda = 2$, L = 0.5 and $\varepsilon = 0.5$ are given in Table 1. After careful observation of $\overline{Nu}$ for each of the chosen grid sizes, an optimum grid size is selected at which the average Nusselt number $\overline{Nu}$ is not varied significantly with a further increment in grids. Also, the utmost variation between 101×101 and 121×121 grids is found within 0.1%, and hence the 101×101 grids are used in all calculations. A code using Fortran is developed for solving the algebraic equations and are compared with the standard benchmark results.

The present results are validated with different benchmark simulations for the limiting cases. First, the simulations are performed for the unit radius ratio case. For $\lambda = 1$, the annular domain reduces to square enclosure. Figure 2a depicts the comparison of streamline and isotherm contours estimated from our simulations and those of Tasnim and Collins [11]. Through this simulation, it has been observed that the current simulations qualitatively agree well with the results of Tasnim and Collins [11]. Next, the simulations for a uniformly heated porous annular geometry without baffle have been obtained and are compared with Shivakumara et al. [27] in Fig. 2b. The comparison reveals a good agreement with the porous annular enclosure in the absence of baffle. Finally, in the absence of baffle, the global Nusselt numbers are determined from present simulations for the Darcy model and are compared with Prasad [26] in a porous annulus. Table 2 reveals an excellent agreement between our predictions and Prasad [26] in the annular cavity without baffle.

4. Results and discussion

Buoyancy-driven convection under the influences of a thin baffle of different lengths positioned at various locations in a vertical porous annulus has been numerically examined. The size and location of baffle has a key role in monitoring the thermal transport, which is the most vital aspects in

(a)

(b)
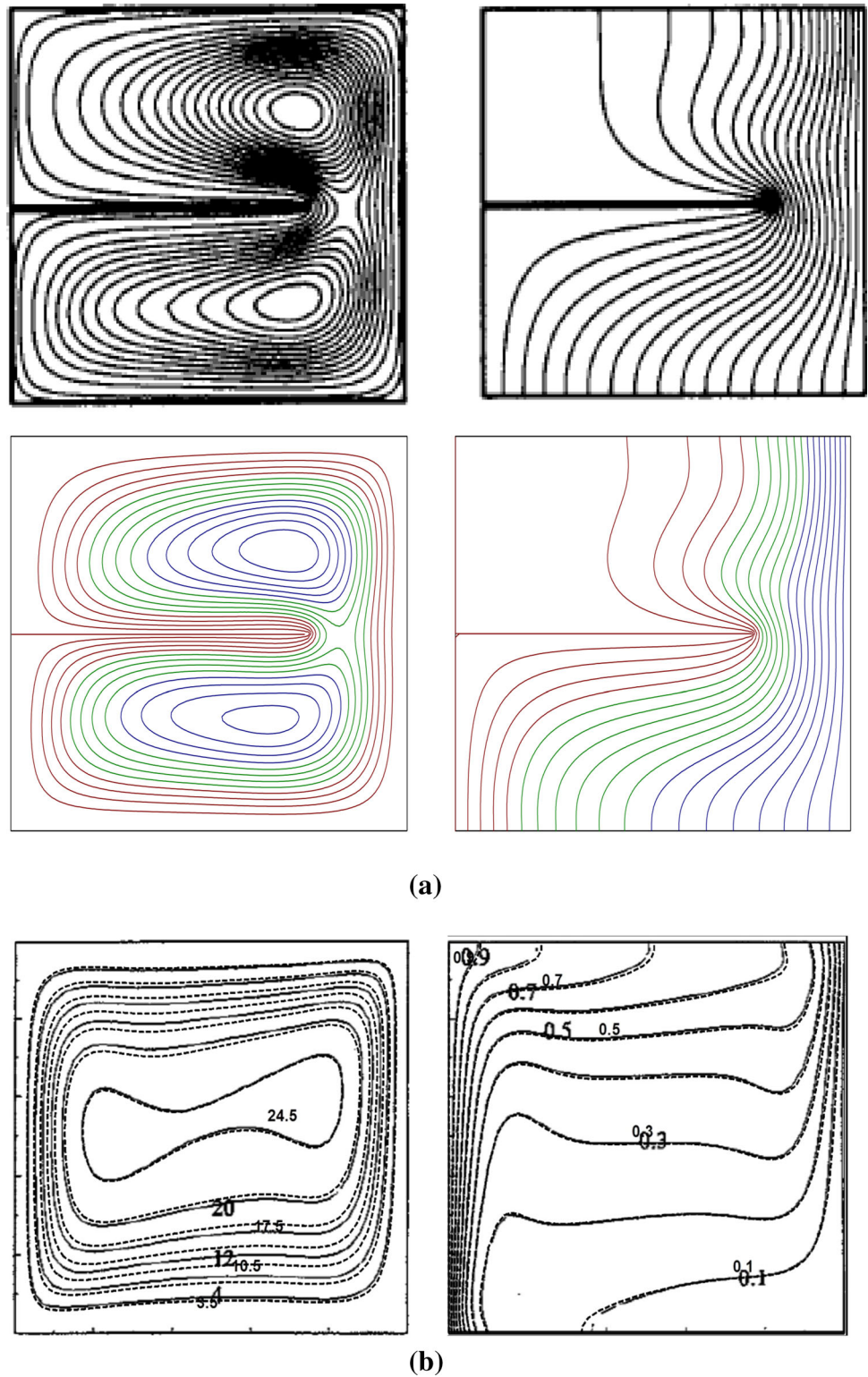
electronic devices. Due to the presence of thermal stress from the temperature variations, the failure of electronic devices increases significantly. As a result, thermal control has been an important component in the design and operation of electronic equipment, which can be achieved by adding fans. But the designers avoid the usage of fans or external devices due to power consumption. However, the addition of a thin baffle could be able to control the

Table 2 Validation of global thermal transport rate with Prasad [26]

Radius ratio (λ)	Darcy-Rayleigh number (Ra_D)	Prasad [26]	Present study	Relative difference (%)
2	10^3	6.4934	6.4815	0.18
	10^4	16.0498	16.0271	0.14
3	10^3	7.1659	7.1804	0.20
	10^4	17.2691	17.2226	0.27
5	10^3	8.0036	8.0262	0.28
	10^4	18.8055	18.8631	0.31
10	10^3	9.3975	9.4452	0.51
	10^4	20.7498	20.8325	0.40

Fig. 3 Rayleigh number impacts on fluid flow (left) and thermal (right) contours for L = 0.5, ε = 0.25, and Da = 10^{-3}. (a) Ra = 10^4, $|\psi_{max}| = 0.8$, (b) Ra = 10^6, $|\psi_{max}| = 17.1$.
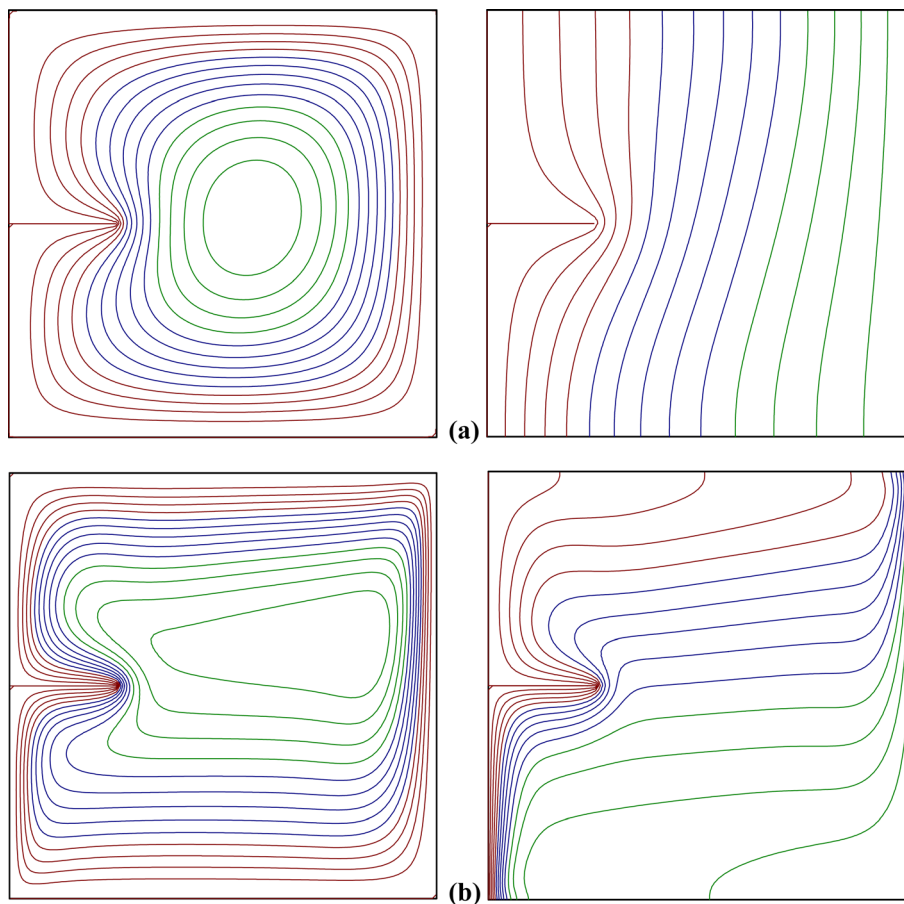
temperature effectively. In particular, determining the optimum size and location of baffle would reduce the failure rate of the electronic devices considerably. In the present analysis, five baffle locations (L = 0.125, 0.25, 0.5, 0.75 and 0.875) and eight baffle lengths (ε = 0.125 to ε = 0.875) are considered. Further, the vast choice of physical parameters, namely Rayleigh (Ra) and Darcy (Da) numbers ($10^3 \leq Ra \leq 10^6$ and $10^{-5} \leq Da \leq 10^{-1}$) are considered for the analysis. However, other parameters such as Pr, A, ϕ and λ are kept, respectively, at Pr = 0.707,

A = 1, ϕ = 0.4 and $\lambda = 2$. The parametric values are carefully chosen to represent the examined physical phenomenon. The range of Rayleigh numbers considered here represents the laminar convective flow regime and the non-dimensional length and location of baffle approximately varied to cover the lengths of baffle used in different types of heat exchangers.

Fig. 4 Darcy number impacts on flow (left) and thermal (right) contours for L = 0.5, ε = 0.25 and Ra = 10^6. (a) Da = 10^{-5}, $|\psi_{max}| = 0.9$,(b) Da = 10^{-3}, $|\psi_{max}| = 17.1$,(c) Da = 10^{-1}, $|\psi_{max}| = 25.7$
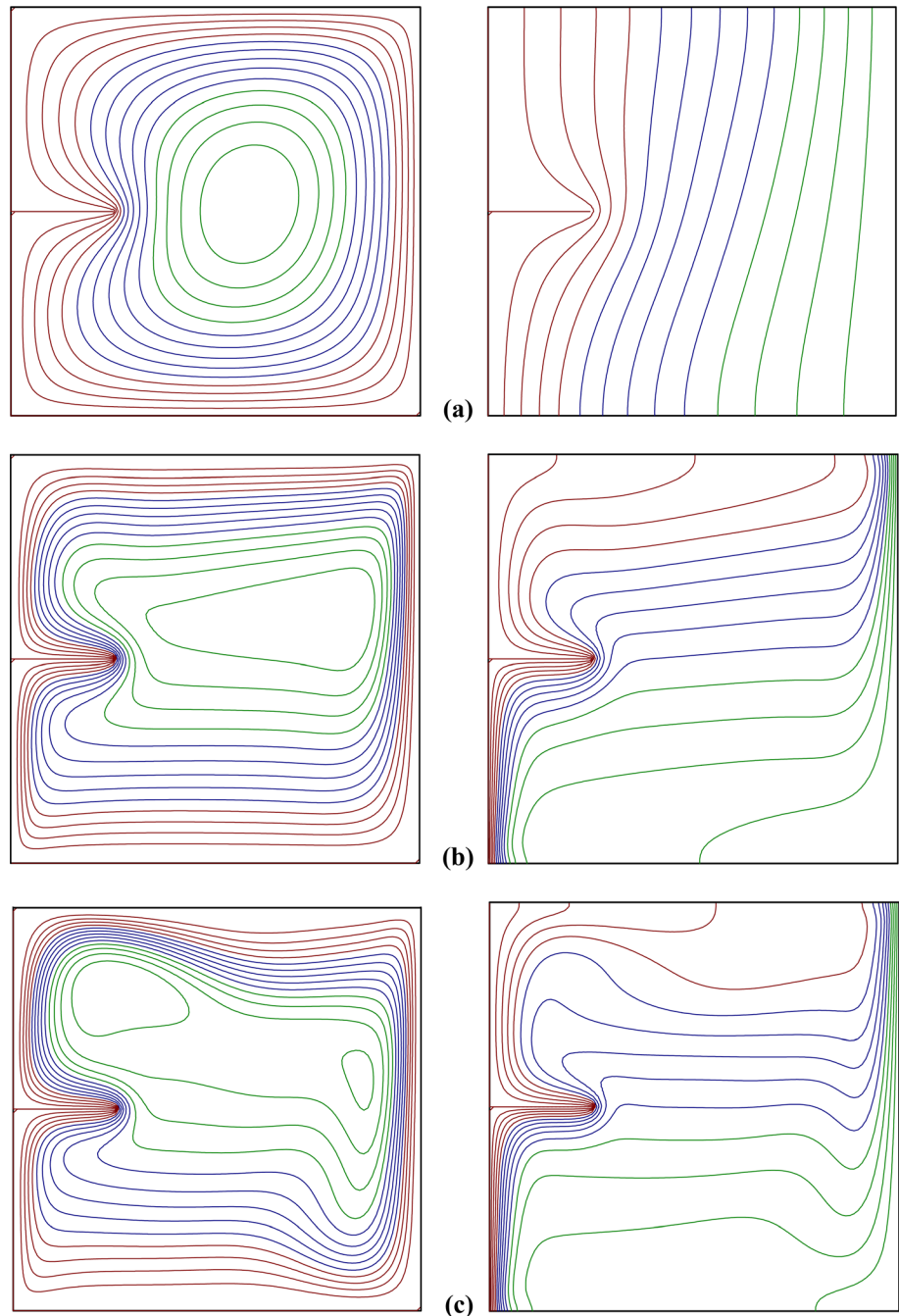

4.1. Effects of fin length and position on flow and temperature fields

The numerical computations are carried out initially for different Rayleigh numbers to comprehend the impact of *Ra* on streamline and isotherm fields by varying Rayleigh number (Ra). Specifically, the baffle location, baffle length and Darcy number are fixed, respectively, at L = 0.5, ε = 0.25 and Da = 10^{-3}. The streamlines and isotherms for the above parameter range are illustrated in Fig. 3. For lower value of Rayleigh number, Ra = 10^4, the fluid parcel

adjacent to hot cylinder rises due to heating and descents alongside the cold cylinder, which results in the formation of a clockwise-rotating vortex in the center portion of annular space. The isotherm contours are nearly parallel to cylindrical surfaces, which reveal that the heat transfer is by conduction. However, once the magnitude of *Ra* is augmented to Ra = 10^6, a drastic variation is observed in the streamlines and isotherms. The main vortex in the streamline contours is elongated horizontally. Also, the streamlines and isotherms are more densely packed near the vertical walls as well as around the baffle. As expected,

Fig. 5 Impact of baffle size on flow (left) and thermal (right) contours for Ra = 10^5, Da = 10^{-2}, L = 0.5, (a) ε = 0.2, $|\psi_{max}|$ = 11.8, (b) ε = 0.5, $|\psi_{max}|$ = 13.1, (c) ε = 0.7, $|\psi_{max}|$ = 13.1
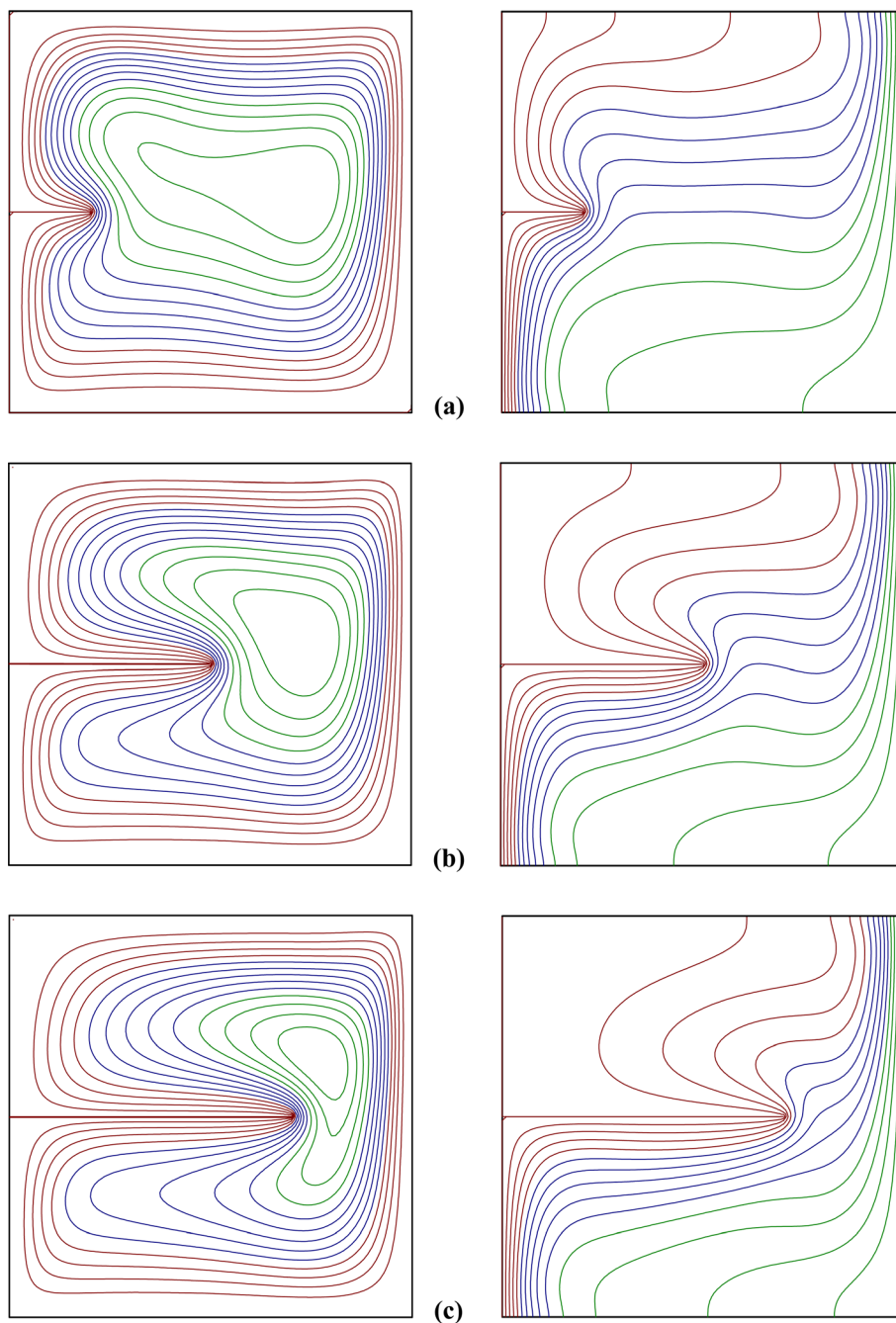
the accelerated fluid motion is observed from the increased buoyant convection at greater values of Ra.

Figure 4 illustrates the influence of Darcy number on the fluid and thermal contours for the fixed values of L = 0.5, ε = 0.25 and Ra = 10^6. It is observed that, for Da = 10^{-5}, the streamlines reveal a slow fluid flow movement due to the presence of densely packed porous media, which is further confirmed through isotherm contours. For higher values of Darcy number, the fluid movement is faster, the deformation of the streamlines and isotherms take place. Also, the primary vortex in the streamlines splits into two vortices and moved near the hot and cold walls. The streamlines are found more densely packed towards the vertical walls, which reveal the convection-dominated fluid flow. It is also confirmed through the magnitude of the maximum stream function, $|\psi_{max}|$, a quantitative measure of flow circulation rate, the flow rates are enhanced by increasing the Darcy number. It has been found that $|\psi_{max}|$ = 0.9, strength of the flow circulation, for Da = 10^{-5} increases significantly to $|\psi_{max}|$ = 17.1 and 25.7 as the Darcy number enhances, respectively, to Da = 10^{-3} and Da = 10^{-1}.

Fig. 6 Baffle location impacts on flow (left) and thermal (right) contours for $\varepsilon = 0.25$, Ra $= 10^5$, and Da $= 10^{-2}$

(a) L $= 0.25$, $|\psi_{max}| = 11.6$

(b) L $= 0.5$, $|\psi_{max}| = 11.5$
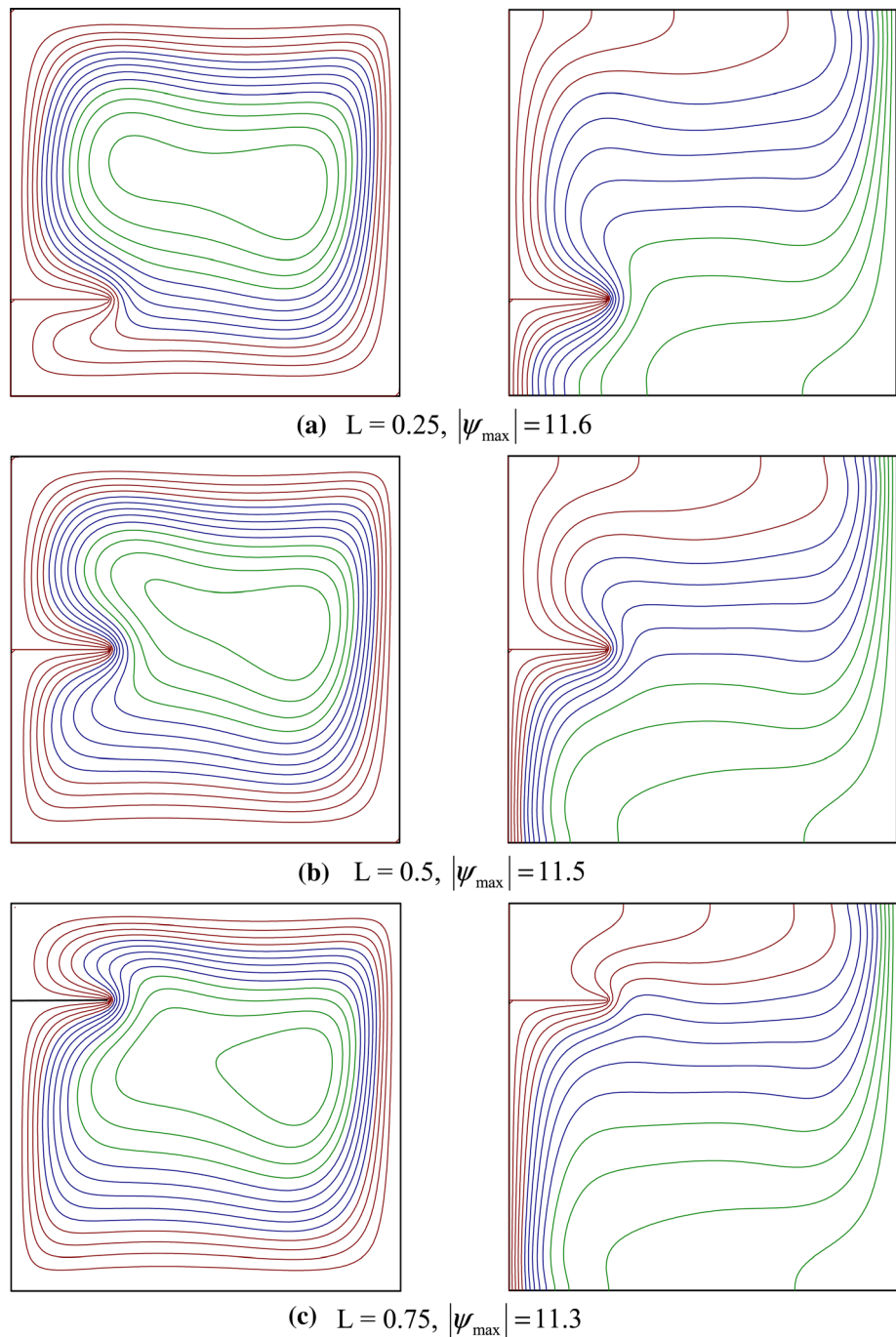
(c) L $= 0.75$, $|\psi_{max}| = 11.3$

Figure 5 depicts the impact of baffle size on flow and temperature fields at constant values of L $= 0.5$, Ra $= 10^5$ and Da $= 10^{-2}$. It is found that for a smaller baffle length $\varepsilon = 0.2$, the streamline contours reveal that the main vortex is slightly elongated diagonally. As the baffle length increases, the streamlines are more compressed towards the outer cold wall and the main vortex moves to the direction of cold wall. The extreme stream function value reveals weaker flow strength at smaller baffle length ($\varepsilon = 0.2$, $|\psi_{max}| = 11.8$). However, an increase in baffle length creates

an upsurge in fluid circulation rate due to the additional thermal energy offered by the baffle ($\varepsilon = 0.7$, $|\psi_{max}| = 13.1$). The isotherm contours illustrate that with reference to the baffle length, isotherms have been transformed to larger extent. For larger baffle length $\varepsilon = 0.7$, the region above the fin is meagerly occupied by isotherm contours, which indicates the fluid motion has been confined to the region below the baffle and creates a motionless flow region or slow-moving flow over the baffle. Figure 6 examines the effect of fin location on flow and
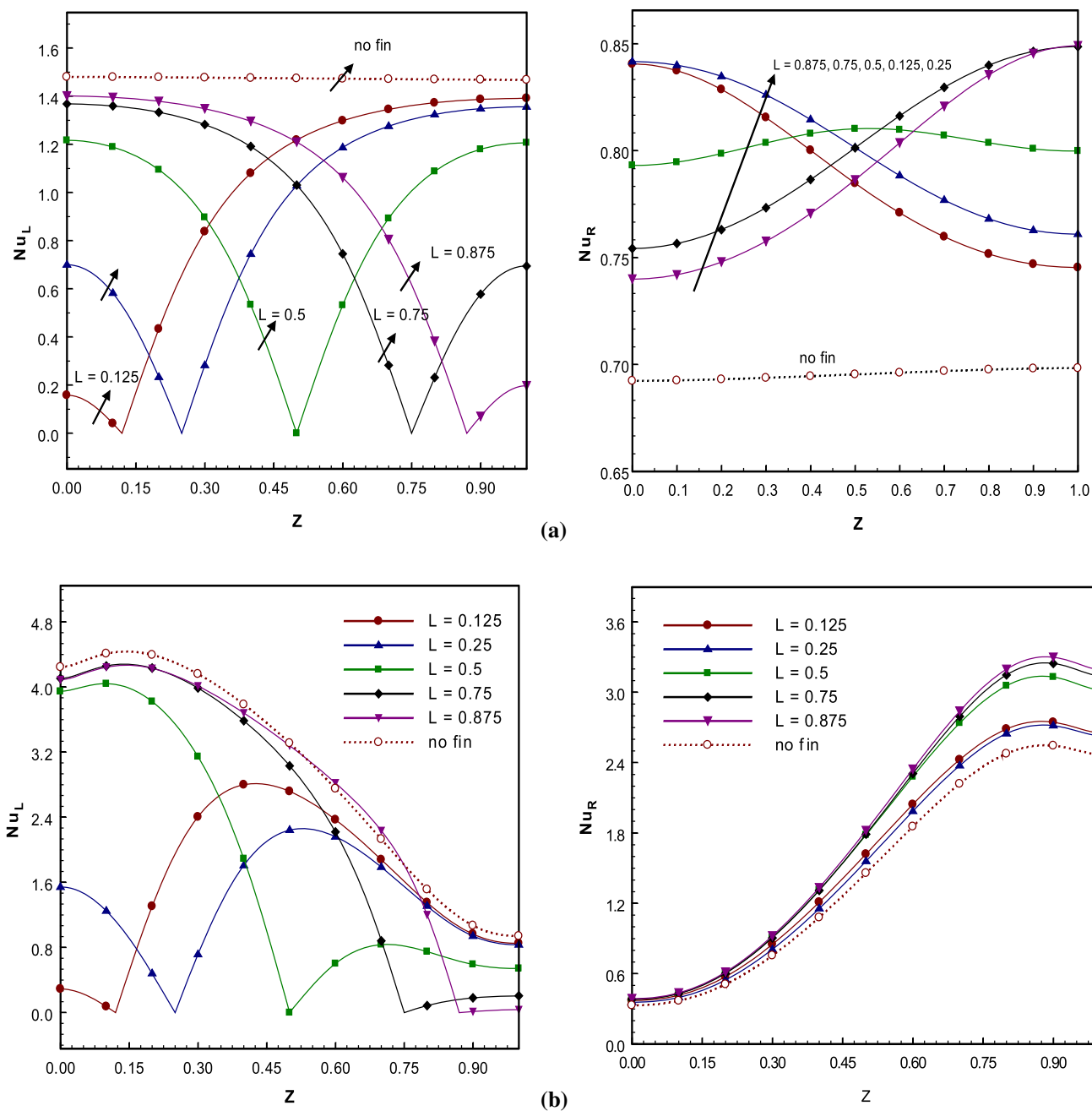
Fig. 7 Local Nu variation over the vertical cylindrical surfaces at Ra = 10^4, and ε = 0.25, (a) Da = 10^{-5} and (b) Da = 10^{-1}

thermal patterns for a smaller baffle length ε = 0.25, Ra = 10^5 and Da = 10^{-2}. For placing the baffle near bottom portion of the annulus, the streamlines are marginally deformed and the primary vertex is elongated diagonally. But, when the baffle is shifted near top, the primary vortex moved towards the outer cylinder and the isotherm contours are not altered to larger extent with reference to the location of the baffle. From the above observations, it is found that the rate of flow movement augments with a rise in baffle size, Darcy and Rayleigh numbers, and declines

with an increase in baffle location and these predictions are physically meaningful. This indicates that the flow movement rate could be efficiently monitored by choosing an appropriate baffle length and position.

4.2. Impact of baffle length and position on heat transport

In this section, we made a detailed examination to comprehend the impacts of Rayleigh number, Darcy number,
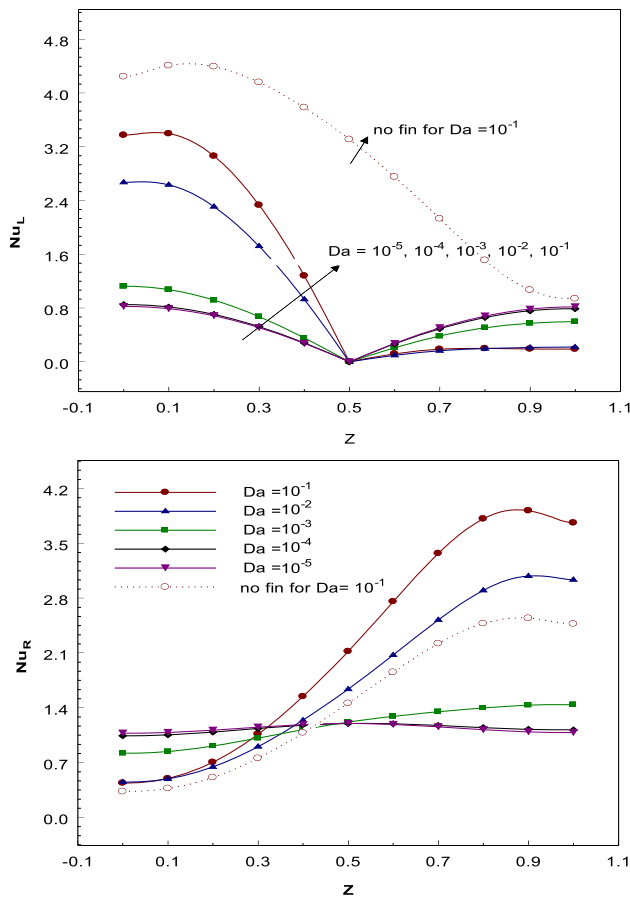
Fig. 8 Local *Nu* variation over the vertical cylindrical surfaces for diverse Darcy numbers and Ra = 10^4, L = 0.5, ε = 0.5

Fig. 9 Local Nu variation over the vertical cylindrical surfaces for diverse fin sizes at L = 0.5, Ra = 10^4, Da = 10^{-5}

Fig. 10 Impact of fin size on global Nusselt number at L = 0.5 and Da = 10^{-2}

baffle length and position on local as well as average thermal transport rates. Figure 7 illustrates the behavior of local *Nu* along the inner (Nu_L) and outer cylinders (Nu_R) for different fin locations (L) and Darcy numbers (Da) by fixing Rayleigh number at 10^4 and baffle length ε = 0.25. The change in Nu_L and Nu_R in the absence of baffle is also estimated for comparison. It is found that the change in local Nusselt number (Nu_L) along the cylindrical walls strongly depends on baffle position and a sharp jump in Nu_L is observed at the baffle location. For Da = 10^{-5}, the local thermal transport rate (Nu_L) decreases steadily underneath the fin and enhances above the fin. The local thermal transport alongside the inner cylinder (Nu_L), above and below the baffle is higher for L = 0.25, which is reverse at the outer wall. The change in local thermal transport rate along the outer wall (Nu_R) increases steadily for L = 0.875 and 0.75 and decreases steadily for L = 0.125 and 0.25, almost flat for L = 0.5. As the Darcy number is raised to Da = 10^{-1}, the local thermal transport rate alongside the outer cylinder steadily increases for every baffle location and is higher for L = 0.875. The local heat transport rate along the inner cylinder is constant
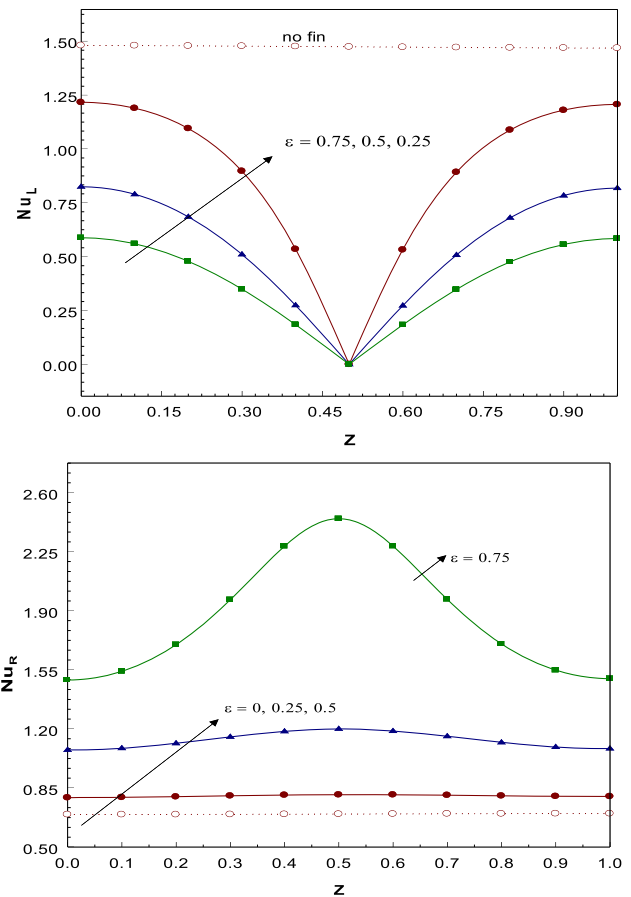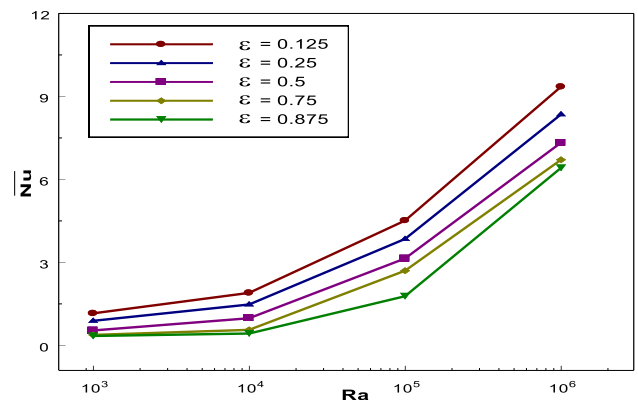
above the baffle for L > 0.5 and in the space beneath the baffle for L < 0.5. It could be expected due to the baffle location near top of the annulus (L = 0.875) causes the restriction of fluid movement to the region below the baffle. As a result, the variation of local *Nu* along the outer wall is higher for L = 0.875.

Figure 8 depicts the variation in local Nu along the inner and outer cylinders for various magnitudes of Da by fixing the values of Ra = 10^4, L = 0.5 and ε = 0.5. The local thermal transfer rates along the inner wall (Nu_L) steadily decreases in the region below the baffle for all Darcy numbers and found to be higher at Da = 10^{-1}. This can be attributed to the drag force offered by the porous medium. The local thermal transport rate Nu_L steadily rises above the baffle for lower Darcy number and does not have much change for the higher Darcy numbers and it is found to be higher for Da = 10^{-5}. The change in local Nu along the outer wall (Nu_R) steadily rises for higher Darcy numbers (Da $\geq 10^{-2}$) and almost flat for lower Darcy numbers. The change in local Nu over the inner and outer cylinders (Nu_L and Nu_R) for three fin sizes ε = 0.25, 0.5, 0.75 by fixing the values of L = 0.5, Ra = 10^4 and Da = 10^{-5} is illustrated in Fig. 9. Further, the local heat transport rate along the outer cylinder (Nu_L) declines steadily below the baffle and enhances gradually above the baffle for all baffle lengths and Nu_L is higher for ε = 0.25 and the variation of local thermal transport rate is reverse at outer cylinder, Nu_R is greater for ε = 0.75 and almost flat for ε = 0.25, 0.5.

In Fig. 10, the influence of fin length on the global thermal transport rate for diverse values of Ra by fixing the magnitude of Da and baffle location is displayed. It is found that as the magnitude of Ra increases, the rate of thermal transfer also increases for any baffle length. This can be expected from the enhancement in Rayleigh number increases buoyant convection, and eventually increases thermal transport rate. From the results pertaining to the impact of fin size on heat transfer rate, it is observed that the global Nusselt number decreases with an increase in baffle length, and heat transfer is higher for smaller baffle length ε = 0.125. Thus, it can be concluded that the baffle behaves like barrier to fluid movement causing a decline in the thermal transport rate. The influence of baffle location on the average Nusselt number for various Rayleigh
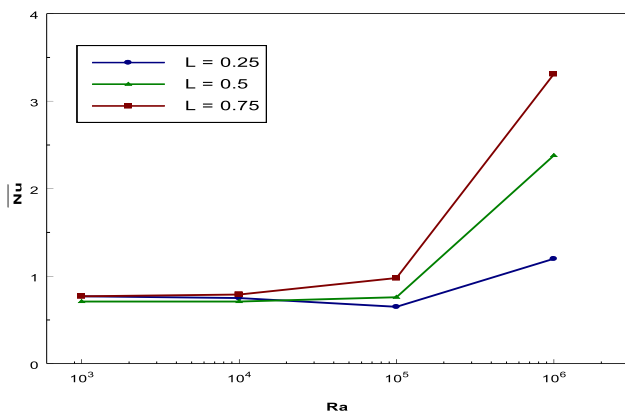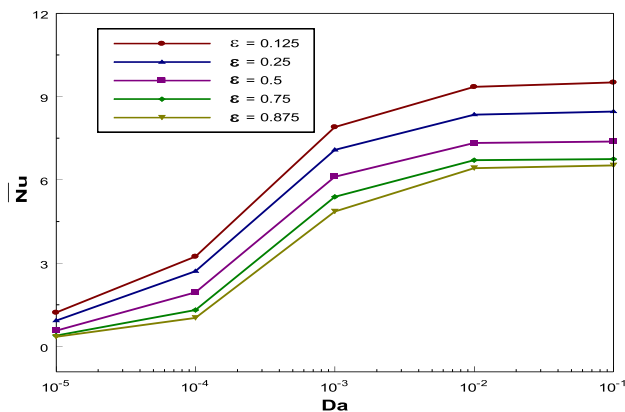

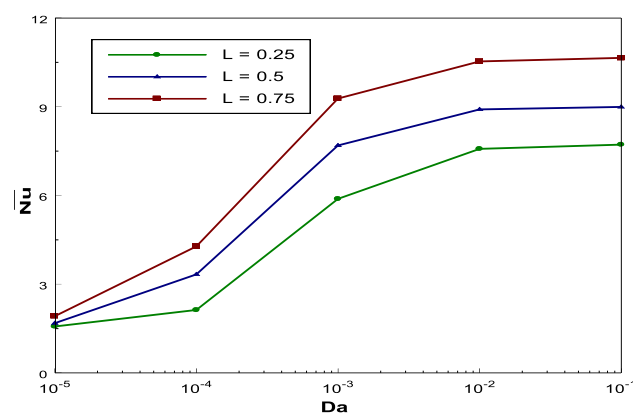**Fig. 12** Effect of fin length and Darcy numbers for Ra = 10^6 and L = 0.5

Fig. 13 Effect of fin location and Darcy numbers for Ra = 10^6 and ε = 0.35

numbers and a fixed value of Da and baffle length (ε) is reported in Fig. 11. It is detected that the energy transport rate increases with increase in the magnitude of Ra and fin position and heat transfer is enhanced for the baffle location near the top of the adiabatic wall L = 0.75.

The baffle length and position impacts on global energy transfer rate for different Darcy numbers at Ra = 10^6 is illustrated through Figs. 12 and 13, respectively. From Fig. 12, it is observed that thermal dissipation rate augments with an upsurge in Da for every fin length. The resistance to the fluid flow reduces with a rise in Darcy number and hence the thermal transport rate increases. Also, the heat transport rate reduces with an increase in baffle length. Higher heat transport rates are achieved with a shorter baffle (ε = 0.125) rather than larger baffle (ε = 0.875). The combined impacts of baffle location and Darcy number on the global transport rate is depicted in Fig. 13. It is found that rate of thermal transmission augments through an upsurge in Darcy number as well as the baffle location. In particular, the heat transport rates are higher when the baffle is located at the top of the cavity.

Fig. 11 Impact of fin location on global Nusselt number for ε = 0.35 and Da = 10^{-4}

From the above observations, it is determined that the thermal transport rate could be enhanced or suppressed by suitable size and location of the baffle and also by varying the Darcy number.

5. Conclusions

In this analysis, numerical simulations are conducted to uncover the impact of baffle length and location on buoyant flow and associated energy transport in an annular domain occupied with porous media. The subsequent conclusions are derived from the findings of numerical simulations:

(1)   The length and position of baffle plays a vital role in altering the flow patterns, temperature fields and thermal transport rates.

(2)   The flow circulation rate increases with an increase in the Rayleigh and Darcy numbers for any baffle length and location.

(3)   The average thermal transport rate enhances through an upsurge in the magnitudes of Ra and Da numbers.

(4)   The heat transport rate could be enhanced or suppressed by choosing an appropriate arrangement of baffle length and location. The rate of heat transport declines as the fin size increases. However, thermal transport rate could be maximized by positioning the baffle nearer to top cylindrical surface.

Author contributions MS formulated the problem and designed code. BVP performed numerical simulations. YD and BVP analyzed the simulations and prepared the manuscript.

Declarations

Conflict of interest The authors declare that they have no conflict of interest.

References

[1]   G de Vahl Davis, RW Thomas, *Physics of Fluids.* **Supplement II**, 198 (1969)

[2]   M Venkatachalappa, M Sankar and A A Natarajan *Acta Mechanica.* **147** 173 (2001)

[3]   F Mebarek-Oudina *Eng. Sci. Technol. Int. J.* **20** 1324 (2017)

[4]   M Sankar, M Venkatachalappa and Y Do *Int. J Heat Fluid Flow.* **32** 402 (2011)

[5]   M Afrand, D Toghraie, A Karimipour and S J Wongwises *J. Magn. Magn. Mater.* **430** 22 (2017)

[6]   M H Hekmat, M B Rabiee and K K Ziarati *J. Therm. Anal. Calorim.* **138** 1745 (2019)

[7]   K Zhang, M Yang and Y Zhang *Int. J Heat Mass Transfer.* **70** 434 (2014)

[8]   M Sankar, S Kemparaju, B M R Prasanna and S Eswaramoorthi *J. Phys.: Conf. Series.* **1139** 1 (2018)

[9]   M Sankar, K Beomseok, J M Lopez and Y Do *Int. J. Heat Mass Transfer.* **55** 4116 (2012)

[10] X Shi and J M Khodadadi Trans. ASME *J. Heat Transfer.* **125** 624 (2003)

[11] S H Tasnim M R Collins *Int. Commun. Heat Mass Transfer.* **31** 639 (2004)

[12] H F Oztop and I Dagtekin A Bahloul *Int. Commun. Heat Mass Transfer.* **31** 121 (2004)

[13] E Bilgen *Int. J Heat Mass Transfer.* **48** 3493 (2005)

[14] A Ben Nakhi, A J Chamkha, *Numeric. Heat Transfer: Part A.* **50**, 381 (2006)

[15] A Ben Nakhi, A J Chamkha, *Int. J. Thermal Sci.* **46**, 467 (2007)

[16] P Kandaswamy, J Lee, A K Abdul Hakeem and S Saravanan *Int. J Heat Mass Transfer.* **51** 1830 (2008)

[17] S Saravanan, A K Abdul Hakeem and P Kandaswamy *Heat Transfer Res.* **40** 805 (2009)

[18] S H Hussain, M Y Jabbar and A S Mohamad *Int. J. Therm. Sci.* **50** 1799 (2011)

[19] P Sriromreun, C Thianpong and P Promvonge *Int. Commun. Heat Mass Transfer.* **39** 945 (2012)

[20] X Wang, D Shi and D Li *Int. J. Heat Mass Transfer.* **55** 8073 (2012)

[21] K Kalidasan, R Velkennedy and P Rajesh Kanna *Int. Commun. Heat Mass Transfer.* **56** 121 (2014)

[22] B V Pushpa, B M R Prasanna, Y Do and M Sankar *J. Phys.: Conf. Series.* **908** 012081 (2017)

[23] N Girish *M Sankar.* (Heat Transfer: O D Makinde) (2020)

[24] D C Reda *Trans. ASME J. Heat Transfer.* **105** 795 (1983)

[25] V Prasad, F A Kulacki and A V Kulkarni *Int. J Heat Mass Transfer.* **29** 713 (1986)

[26] V Prasad *Int. J. Heat Mass Transfer.* **29** 841 (1986)

[27] I S Shivakumara, B M R Prasanna, N Rudraiah and M Venkatachalappa *J. Porous Media.* **5** 87 (2003)

[28] M Sankar, Y Park, J M Lopez and Y Do *Int. J Heat Mass Transfer.* **54** 1493 (2011)

[29] H Olfian, AZ Sheshpoli, SSM Ajarostaghi, *Heat Transfer — Asian Res.* (2020)

[30] TR Mahapatra, D Pal, S Mondal, *Int. J. of Appl. Math. Comput.* **4** 359 (2012)

[31] T R Mahapatra, D Pal and S Mondal *Nonlinear Anal.: Model. Control* **17** 2 223 (2012)

[32] M Sankar, B Jang and Y Do *J. Porous Media.* **17** 373 (2014)

[33] TR Mahapatra, D Pal, S Mondal, *Int. J. of Appl. Math. Mech.* **9(13)**, 23 (2013)

[34] S Mondal, T R Mahapatra and D Pal *Int. J. Mech. Eng. Technol.* **3** 3 187 (2012)

[35] T R Mahapatra, D Pal and S Mondal *Int. J. Nonlinear Sci.* **11** 3 366 (2011)

[36] B M Al-Srayyih, S Gao and S H Hussain *Phys. Fluids.* **31** 043609 (2019)

[37] T D Manh, I Tlili, A Shafee, T Nguyen-Thoi and H Hamouda *Phys. A: Stat. Mech. Appl.* **554** 123940 (2020)

[38] M Izadi, M A Sheremet and S A M Mehryan *Chin. J. Phys.* **65** 447 (2020)

[39] S Mondal and P Sibanda *Int. J. Heat Mass Transfer.* **85** 401 (2015)

[40] Y Varol, H F Oztop and A Varol *Int. J. Therm. Sci.* **46** 1033 (2007)

[41] K Khanafer A Al Amiri, J Bull *Int. J Heat Mass Transfer.* **87** 59 (2015)

[42] P Promvonge and S Skullong *Int. J Therm. Sciences.* **155** 106429 (2020)

[43] R Y Farsani, A Mahmoudi and M Jahangiri *Therm. Sci. Eng. Progress.* **16** 100453 (2020)

[44] H R Abbasi, E S Sadeh, H Pourrahmani and M H Mohammadi *Appl. Therm. Eng.* **180** 115835 (2020)

[45] X Cao, D Chen, T Du, Z Liu and S Ji *Int. J. Heat Mass Transfer.* **160** 120181 (2020)

[46] S A M Mehryan, A Alsabery, A Modir, E Izadpanahi and M Ghalambaz *Int. J. Therm. Sci.* **153** 106340 (2020)

[47] B V Pushpa, M Sankar and O D Makinde *Therm. Sci. Eng. Progress.* **20** 100735 (2020)

[48] L Wang, W W Wang, Y Cai, D Liu and F Y Zhao *Numeric. Heat Transfer. Part A: Appl.* **77** 361 (2020)

[49] T Salahuddin, M Arshad, N Siddique, I Tlili, *Indian J. Phys.* (2020). https://doi.org/10.1007/s12648-020-01833-0